Progress In Electromagnetics Research, PIER 85, 393–408, 2008

A POLARIZATION COMPENSATION APPROACH UTILIZING A PARABOLOID PHOTONIC-CRYSTAL STRUCTURE FOR CROSSED-DIPOLE EXCITED REFLECTOR ANTENNAS

B. Li

Key Laboratory of Optical Communication and Lightwave Technologies, Ministry of Education
Beijing University of Posts and Telecommunications
China

K.-J. Lee

Department of Communication Engineering
Oriental Institute of Technology
Taiwan, R.O.C

H.-T. Chou

Department of Communications Engineering
Yuan Ze University
Taiwan, R.O.C.

W. Gu

Key Laboratory of Optical Communication and Lightwave Technologies, Ministry of Education
Beijing University of Posts and Telecommunications
China

Abstract—An approach utilizing a paraboloid photonic crystal structure (PPCS) is proposed in this paper to compensate the polarization discrimination of an antenna's radiation. It is demonstrated by considering a reflector antenna excited by a pair of crossed-dipoles, whose circularly polarized (CP) radiation may be distorted due to the scattering from the finite reflector surface. The proposed approach tends to compensate the discrimination and achieve a wider beamwidth of good axial ratios while, in the mean time, retaining a less gain loss. The advantage of this approach is that

the PPCS can be integrated into a radome structure of the antenna without increasing an excess cost. Numerical studies are conducted in this paper and demonstrate that this compensation method can achieve a beamwidth of about 30 degrees at the frequency of 12.45 GHz.

1. INTRODUCTION

Reflector antennas have been shown wide applications such as in the Ultra Wide-Band (UWB) communication and radar applications in recent years [1–4]. Among these applications, antenna radiation with good circular polarizations (CP) is one of the important interested designs in practical applications. However, due to the finite size and shape of the reflecting surface, the performance of the CP radiation may experience degradation as the feed's radiation scatters from the reflecting surface [5–8]. This polarization discrimination of TE and TM modes, which corresponds to the two orthogonal components of the CP fields, grows while the angle of incident waves increased with respect to the antenna's boresite [9]. This discrimination especially increases at high frequencies as the surface distortion increases rapidly in terms of wavelength, where a RMS surface accuracy of less than 1.5 mm is generally required if a high antenna efficiency is to be achieved [10]. This high accuracy is potentially difficult to achieve in practical manufactures. It is thus important to develop techniques to compensate this CP discrimination.

This paper presents a useful and promising approach utilizing a photonic crystal structure. This approach has an advantage that it may be integrated into the design of a radome structure for the original antenna without increasing excess costs. In this paper, a popular radome shape of a paraboloidal structure is considered to demonstrate its applications, which is designed using the proposed crystal structure. The concepts of the photonic crystals [11–14] were first brought forward by Yablonovitch [15] and John [16] and are now widely used in the newly emerged area of integrate optics and many kinds of sensors [17]. It was shown in Optics that if the structures have a periodicity in the range of the wavelength of the light, interferences appear, which affect the propagation of light in these materials strongly and allow the energy re-distributing in the angular space. Thus the different mechanisms of energy re-distribution in the TE and TM modes may be used to make their ratio become smaller if the structure is designed properly because at high frequencies the radio waves have characteristics of propagation similar to ray optics. This concept can be used to compensate the CP radiation and broaden the beamwidth

of low axial ratio as proposed here.

This paper is formatted in the following order. Section 2 describes the proposed approach. Especially the reflector antenna is assumed to be fed by a pair of crossed-dipoles that is a classical approach to radiate CP fields in practical applications. Section 3 describes environments and parameters used in the simulation studies. The parameters of the proposed PPCS design are also described. Numerical studies, as well as examples, to validate the concepts are presented in Section 4. Finally some discussions are presented in Section 5 as a conclusion to this work.

2. THE REFLECTOR ANTENNA AND POLARIZATION COMPENSATION APPROACH

The proposed structure under examination is illustrated in Figure 1, where the bottom is a reflector antenna fed by a feeding antenna to radiate a CP electromagnetic fields. The top portion in Figure

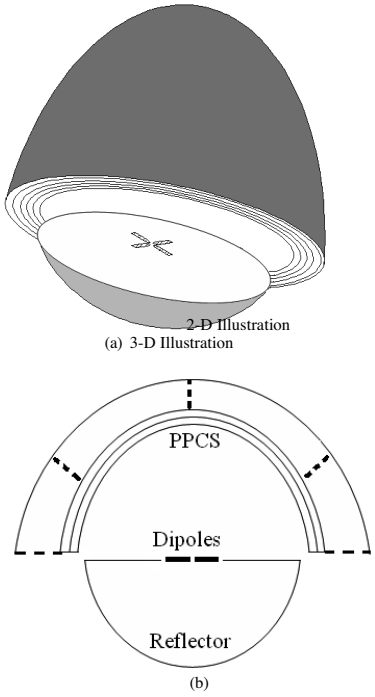

Figure 1. Integrated antenna and radome structure under study. The bottom portion is the reflector antenna while the top portion illustrates a PPCS.

1 exhibits a PPCS proposed to compensate CP discriminations. Reflector antennas serve here as demonstrating examples. The PPCS may also be applied to other antennas in a similar fashion, which is omitted for brevity of this paper.

2.1. Radiation Analysis of Reflector Antennas

For simplity, the reflector antenna under examination is a parabola of revolution about the z-axis as shown at the bottom portion of Figure 1. Its radiation characteristics may be analyzed using the concepts of ray tracing as illustrated in Figure 2 [14, 17]. The fields radiated from a feed, which is assumed to be placed at the focus of the reflector to radiate focused beam, will experience reflections from the reflector surface, and diffractions from surface's edges. In a practical analysis, it may be approximated by computing the fields, $(\overline{E}_A, \overline{H}_A)$, on the open aperture of the reflector using ray tracing of Geometrical Optics (GO). Its radiations can be found by using the radiation integral

$$\begin{aligned}\overline{E}(\overline{r}) \cong & \frac{jk}{4\pi} Z_0 \iint\limits_S \hat{R} \times \hat{R} \times \overline{J}(\overline{r}') \frac{e^{-jkR}}{R} ds' \\ & + \frac{jk}{4\pi} \iint\limits_S \hat{R} \times \overline{M}(\overline{r}') \frac{e^{-jkR}}{R} ds' \end{aligned} \tag{1}$$

where the equivalent currents are defined by $\overline{J}(\overline{r}') = \hat{n} \times \overline{H}_A(r')$ and $\overline{M}(\overline{r}') = \overline{E}_A(r') \times \hat{n}$ with $\hat{n}$ being the outward unit surface normal vector at the aperture.

A ray tracing path is shown in Figure 2, where due to its symmetry φ variable is ignored, O is the focal point, and P is an arbitrary point on the surface of the reflector. The ray launched from O experiences a reflection from the reflector surface at P and reaches an aperture at Q. The aperture is formed by the reflector normally projected to the plane consisting of the focal point and parallel to x-y plane. In Figure 2, $\hat{r}$ is the radial unit vector and $\hat{n}$ is the normal unit vector at Q. Note that for an ideal paraboloidal surface the reflected ray propagates in parallel to z-axis passing through P and Q, which can be shown [17] by the trait of the parabola determined by $|OP| + |PQ| = 2f$, where f is the focus length. It reduces to $r = 2f/(1 + \cos\theta) = f\sec^2(\theta/2)$. Using $\hat{n} = -\hat{a}_r \cos(\theta/2) + \hat{a}_\theta \sin(\theta/2)$ and Snell's law of reflection, it can be shown that

$$\cos\alpha_1 = -\hat{a}_r \cdot \hat{n} = \cos(\theta/2) \tag{2}$$

$$\cos\alpha_2 = -\hat{a}_n \cdot \hat{n} = \cos(\theta/2). \tag{3}$$

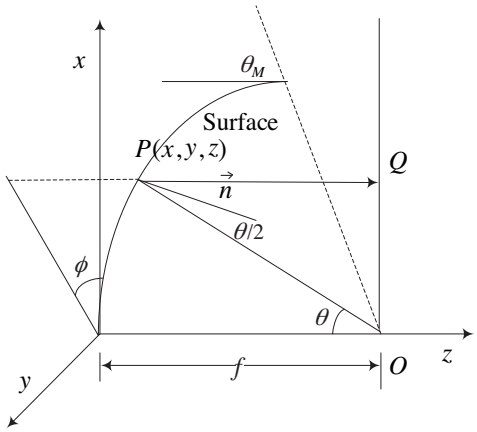

Figure 2. Ray tracing on the paraboloidal reflector.

Thus if the feed is located at the focal point, all reflected rays propagates in parallel at the aperture and produce an in-phase field distribution on the aperture [18–20]. If the feed has ideal CP radiations, the aperture fields will theoretically produce good CP radiations when the aperture is extended to infinity because the asymptotic evaluation of (1) will reduce to GO ray fields of plane waves [17].

In reality, the CP radiation degrades for the following reasons. First, the finite aperture size (corresponding to a finite reflector size) will rise edge diffractions to contaminate the CP radiation, whose effects are apparent if the reflector is not very large. Second, the distortion of the reflector surface caused in the procedure of manufacture will deviate the reflected rays from propagating in parallel. This deviation distorts the polarization of the field distribution on the aperture and thus in turn degrades the CP radiation. Third, a reflector tends to concentrate the energy of feed's radiation. Realistic feeds have good CP radiations only near feeds' boresite directions. The CP performance deviates increasingly as the angles of radiation deviate off the boresite directions. These CP degradations will pollute the CP of the field distribution on the aperture. In general, the CP radiation of the reflector antenna degrades rapidly as the radiation angles are off the antenna boresite.

The gain will also degrade, too. Assuming a feed without loss and reflector being in the far zone of the feed, (1) may result in the

following equations to find the gain [17]:

$$G = 2\cot\frac{\theta_M}{2}\left[\int_0^{\theta_M} f_E(\theta)\tan\frac{\theta}{2}d\theta\right]^2 \Big/ \left(\int_0^{\theta_M} f_P^2(\theta)\sin\theta d\theta\right) \quad (4)$$

where the patterns inside the integrals are related to feed's patterns by

$$f_E(\theta) = \frac{R_{\mathrm{TE/TM}}+1}{4\pi\sqrt{(R_{\mathrm{TE/TM}}+1)^2+(R_{\mathrm{TE/TM}}-1)^2}}\int_0^{2\pi}\left\{\left[\left|\frac{f_\theta(\theta,\phi)}{f_\theta^0(\theta,\phi)}\right| + \left|\frac{f_\phi(\theta,\phi)}{f_\phi^0(\theta,\phi)}\right|\right]e^{j\gamma} + \frac{R_{\mathrm{TE/TM}}-1}{R_{\mathrm{TE/TM}}+1}\left[\left|\frac{f_\theta(\theta,\phi)}{f_\theta^0(\theta,\phi)}\right| - \left|\frac{f_\phi(\theta,\phi)}{f_\phi^0(\theta,\phi)}\right|\right]e^{-j(\gamma-2\phi)}\right\}d\phi, \quad (5)$$

$$f_P^2(\theta) = \frac{1}{4\pi}\int_0^{2\pi}\left\{\left|\frac{f_\theta(\theta,\phi)}{f_\theta^0(\theta,\phi)}\right|^2 + \left|\frac{f_\phi(\theta,\phi)}{f_\phi^0(\theta,\phi)}\right|^2 + \frac{R_{\mathrm{TE/TM}}^2-1}{R_{\mathrm{TE/TM}}^2+1}\cos 2(\gamma-\phi)\left[\left|\frac{f_\theta(\theta,\phi)}{f_\theta^0(\theta,\phi)}\right|^2 - \left|\frac{f_\phi(\theta,\phi)}{f_\phi^0(\theta,\phi)}\right|^2\right]\right\}d\phi \quad (6)$$

with $f_\theta(\theta,\phi)$ and $f_\theta(\theta,\phi)$ being the radiation patterns of the crossed-dipoles. Its maximum values at boresite are

$$f_\theta^0(\theta,\phi) = \frac{\sqrt{2}}{\sqrt{R_{\mathrm{TE/TM}}^2+1}}[R_{\mathrm{TE/TM}}\cos(\gamma+\phi)+j\sin(\gamma-\phi)] \quad (7)$$

$$f_\phi^0(\theta,\phi) = \frac{\sqrt{2}}{\sqrt{R_{\mathrm{TE/TM}}^2+1}}[R_{\mathrm{TE/TM}}\sin(\gamma+\phi)+j\cos(\gamma-\phi)]. \quad (8)$$

$f_\phi(\theta,\phi)$ and $f_\theta(\theta,\phi)$ in (5) and (6) are normalized by their maxima. In (5)–(8), $R_{TE/TM}$ is the excitation ratio of the crossed-dipoles, and γ is a reference angle for dipole's orientation with respect to $\phi = 0^\circ$. Thus (7) and (8) exhibits ideal CP radiations at $\theta = 0^\circ$ if $R_{TE/TM} = 1$

2.2. The Proposed Compensation Approach

The CP degradation of the reflector antenna is compensated by using a PPCS that is developed utilizing a multi-layered substrate. The formation of the layers exhibits periodicity using dielectric materials that can be recognized as multilayer films printed on a bottom dielectric substrate [5, 21, 22]. The full-wave analysis of the printed conductors, consisting of multilayered array of patches in a stratified dielectric medium, has been proposed, but it is still computationally heavy [23–26]. The different mechanisms of energy re-distribution in the TE and TM modes may be used to make their ratio become smaller if the structure is designed properly because at high frequencies the radio waves have characteristics of propagation similar to ray optics. Based on the KP (Kronig-Penney) model [9], we design PPCS with the values of permittivity in a ABAB alternative form materialsas can be seen in Figure 3.

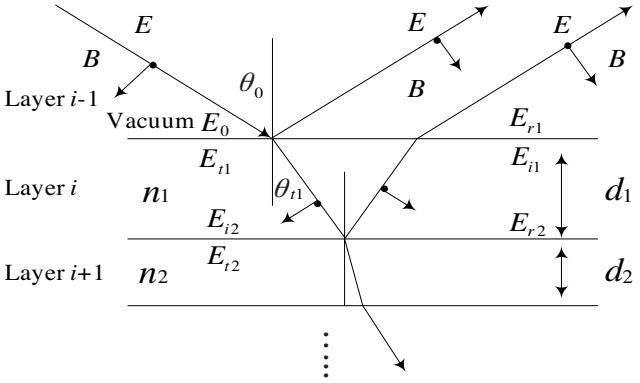

Figure 3. Reflection and transmission in a PPCS.

Figure 3 is a planar multi-layered substrate to illustrate the wave propagation through a PPCS, which is to approximate the PPCS in the local vicinity of a point where the fields radiated from the parabolic reflector illuminate the PPCS. Thus using the boundary condition that the tangential components of the resultant E- and H-field are continuous across the interface and their magnitudes on either side are equal. Under this restriction of the boundary condition [27], we get the relation of the electric and magnetic fields between the adjacent layers of the crystal:

$$\begin{bmatrix} E_k \\ B_k \end{bmatrix} = \begin{bmatrix} \cos\delta_k & i\sin\delta_k/\gamma_k \\ i\gamma_k \sin\delta_k & \cos\delta_k \end{bmatrix} \begin{bmatrix} E_{k+1} \\ B_{k+1} \end{bmatrix} \tag{9}$$

where $\delta_k = \frac{2\pi}{\lambda} n_k d_k \cos\theta_k$, $1 \le k \le N$, $\gamma_k = n_k \sqrt{\mu_0 \varepsilon_0} \cos\theta_{tk}$. In (9), E_k is consisted of E_{tk} and E_{ik} as shown in Figure 3. Let M_k denote the 2×2 matrix on the right hand side of (9), the overall relation between the fields external to the substrate can be described as

$$\begin{bmatrix} E_1 \\ B_1 \end{bmatrix} = M \begin{bmatrix} E_N \\ B_N \end{bmatrix} \tag{10}$$

where M is the compound matrix and $M = M_1 M_2 \ldots M_N$. M-matrix is generally represented in the following form:

$$M = \begin{bmatrix} m_{11} & m_{12} \\ m_{21} & m_{22} \end{bmatrix} \tag{11}$$

The reflection and transmission coefficients are defined as:

$$r = E_{r1}/E_0 \quad \text{and} \quad t = E_{tN}/E_0 \tag{12}$$

Substituting the expression of t, r, and M in (11) and (12) into the boundary condition, (10) can be solved for the transmission and reflection coefficients in terms of the transfer-matrix elements to give:

$$t = \frac{2\gamma_0}{\gamma_0 m_{11} + \gamma_0 \gamma_s m_{12} + m_{21} + \gamma_s m_{22}} \tag{13}$$

$$r = \frac{\gamma_0 m_{11} + \gamma_0 \gamma_s m_{12} - m_{21} - \gamma_s m_{22}}{\gamma_0 m_{11} + \gamma_0 \gamma_s m_{12} + m_{21} + \gamma_s m_{22}} \tag{14}$$

Equations (9)–(14) allows one to find the transmitted fields on the external surface of PPCS. In a practical design, it is desired to maximize the transmission coefficients such that most of the energy will penetrate through PPCS and radiates into the space.

3. SIMULATION ENVIRONMENTS AND PPCS DESIGN

The implementation of this PPCS is shown in Figure 1, which has a 72 mm diameter and 18 mm height. One monopole's length of the crossed-dipoles is 3.6 mm, the inner width is 0.3 mm, and the outer width is 0.8 mm, which is printed on a FR4 substrate and is used as a feed to the reflector antenna. The focal length of the reflector is a quarter of wave length in a free space at 12.45 GHz. Crossed dipoles are used here because they exhibit good CP radiations at the boresite and on the two orthogonal angular planes. Deviated from these planes, the CP radiation starts to degrade, and thus they can be used to illustrate the third case mentioned in the third paragraph of Section 2.1. Also

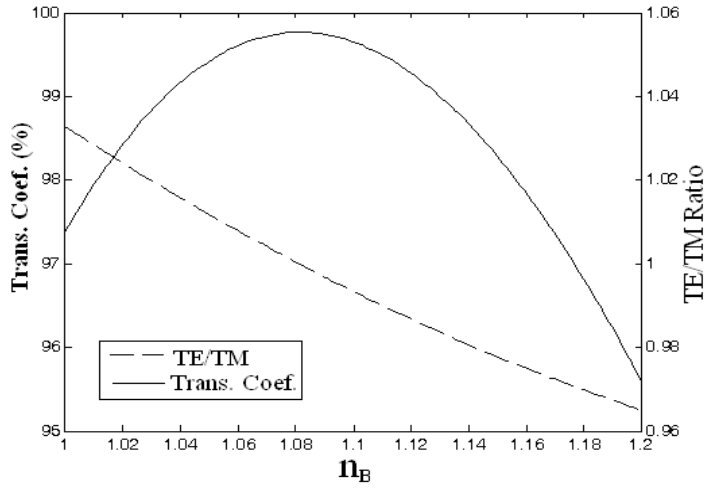

Figure 4. Transmission coefficients and TE/TM ratio of a PPCS.

the reflector's size is comparable with the feed's size, thus the edge diffracted fields may contaminate the CP radiation.

The PPCS is designed using a 4-layer substrate with the values of relative permittivity in an ABAB alternative form. A glass substrate is used at the top of the PPCS and fields are assumed to be incident from air ($n_0 = 1$). The values of relative permittivity of the 4 layers below the glass substrate are determined by maximizing (13) using (9)–(13) that implies most energy transfer into space. The incident fields are assumed to be a plane wave propagating through the substrate at various angles since a focus fed parabolic reflector produces a planar wavefront in the near zone where PPCS is located. The largest angle is selected that most of the energy penetrates through PPCS. The determination requires intensive numerical examinations to search for most appropriate values. However, Figure 4 shows an example of the transmission coefficient and TE/TM ratio with respect to the refraction index, n_B, of layer B where $n_A = 1.2$ and the refraction index of glass is $n_S = 1.52$. In this case the incident angle is 30 degrees, and it is found that the thickness of each layer is approximately $\lambda/4$, where λ is the effective wavelength of the substrate at 12.45 GHz. As shown in Figure 4 that the transmission coefficient has a maximum value at $n_B = 1.08$, and the TE/TM ratio is nearly equal to one within a difference of ± 0.04. Thus in the following examination, the values of relative permittivity are selected by 1.44, 1.172, 1.44 and1.172, respectively (which correspond to refraction index of 1.2 and 1.08,

respectively) while the relative permeability of all the layers is 1. Each layer has a thickness of a quarter of effective wavelength at 12.45GHz. All the films are assumed to be both homogeneous and isotropic.

In the numerical simulation, a finite element method (FEM) based commercial code, HFSS, developed by Ansoft is used, where perfectly matched layers (PMLs) are assumed to fully absorb the electromagnetic fields impinging upon them and thus simulate the antenna radiation in a free space. This tool had been widely used and validated to be very accurate in this type of antenna simulation. Thus without going through experimental measurement, the following numerical results can be believed to be reliable. To justify the performance of this compensation approach, a 3 dB beamwidth is defined to satisfy

$$20|\log(\mathrm{TE}/\mathrm{TM})| < 3\,\mathrm{dB} \tag{15}$$

In a angular space, the beamwidth is determined by the angles between $\theta_{\min}$ and $\theta_{\max}$, within which (15) is satisfied. In particular, $\theta_{\min}$ is the minimal angle of patterns and $\theta_{\max}$ is the maximal angle. As mentioned in Section 1, the goal is to widen this 3 dB beamwidth and thus enhance the antenna performance.

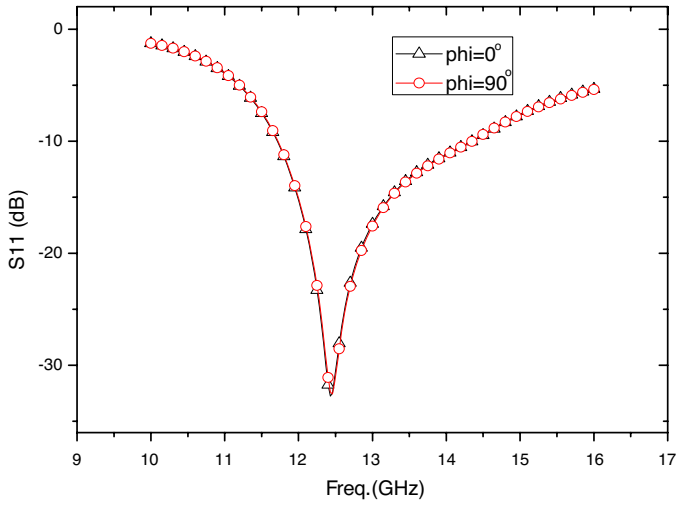

Figure 5. The reflection coefficients of the crossed dipoles with the presence of a paraboloidal reflector.

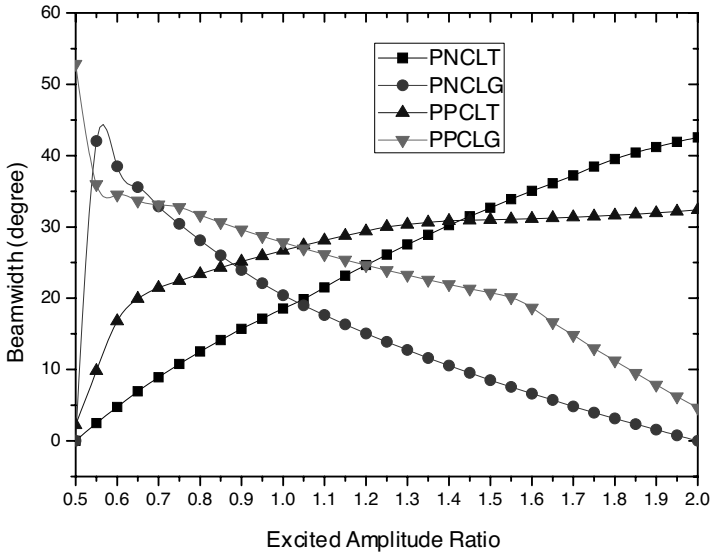

Figure 6. The beamwidth with a different excited amplitude ratio.

4. NUMERICAL RESULTS

The analysis sweeps the frequency from 10 GHz to 15 GHz by 201 sampling points. First, the reflection coefficients of the pair of orthogonally crossed dipoles that excite the paraboloidal reflector are shown in Figure 5, which shows good behaviors of operation at Ku-band with this additional photonic crystal structure. It shows that the placement of this additional photonic crystal structure does not incur problems on the dipoles' radiations.

Next, the variations of beamwidths are shown in Figure 6, where the four curves are obtained by two scenarios, i.e., by taking the -3 dB beamwidths using (15) from the crossed-dipole excited reflector antenna's radiations with and without the implementation of the polarization compensation (indicated by "PPC" and "PNC", respectively). In Figure 6, "LT" and "LG" denote the radiations at latitude and longitude directions, respectively (i.e., radiations at the two principal planes of 0 and 90 degrees, respectively). The amplitude ratio between the two dipoles' excitations serves as a freedom to achieve a good performance, which is labelled on the horizontal axis in Figure 6. Several phenomena are observed. First, as the dipoles are nearly equal excited (At the ratio of 1.05, the maximum beamwidth appears), the radiation patterns at the two principal planes have same beamwidths

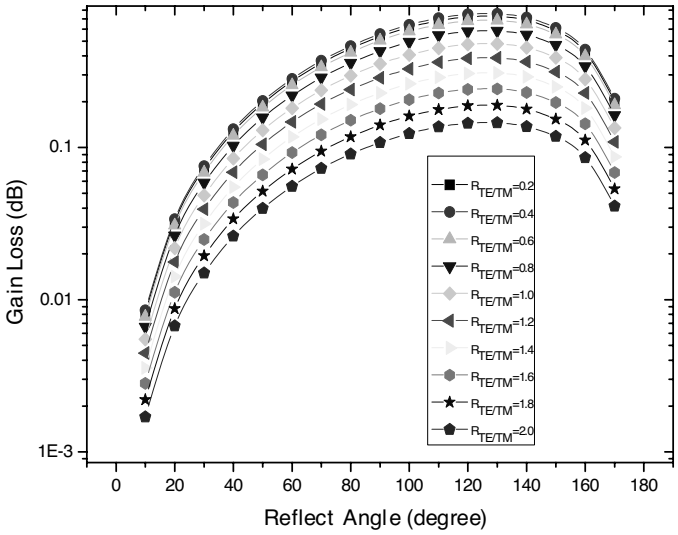

Figure 7. Gain loss vs. reflection angle.

of axial ratio due to the symmetry of the entire antenna structure. However, as shown in Figure 5, the placement of this photonic-crystal structure has significantly increased the beamwidth from 19 degrees to 29 degrees, which indicates a 50% enhancement. It was indicated from numerical experience that this compensation method may averagely achieve more than 35% improvement in comparison with that without any compensation. Secondly, after the compensation the curves also change more smoothly with smaller slopes regarding to the changes of excitation ratio that may occur in the manufacture procedure, which makes it attractive in the applications of long-haul communications.

The gain loss (GL) is shown in Figure 7 for different reflectors' span angles, θ_M, defined in Figure 2, ranged from 10 degrees to 170 degrees. It is noted that θ_M is directly related to the ratio of focal length and diameter of a reflector. It may be used to justify GL for a variety of reflector antennas under this scenario. Also $R_{\mathrm{TE/TM}}$ represents the amplitude ratio of the crossed dipoles' excitions. GL increases as θ_M increases until it reaches 120 degree. After that the curves of GL decreases. GL decreases by 0.1 dB with every 20% increase in $R_{\mathrm{TE/TM}}$ while $R_{\mathrm{TE/TM}} > 0.4$. The case that results in most severe gain losses is shown by the top curve that reaches a highest GL of 0.756 dB at 130 degrees, where $R_{\mathrm{TE/TM}} = 0.4$. GL decreases rapidly while θ_M is larger than 140 degree.

The gain variation (GV) is depicted in Figure 8, which considers

the gains due to the change of dipoles' excitation ratio. GV is obtained by comparing the gain losses shown in Figure 7 with the case that uses an unity excitation ratio. The maximum GV is 60% while $R_{\mathrm{TE/TM}}$ is 0.3. After that maximum value, GV decreases as $R_{\mathrm{TE/TM}}$ grows. θ_M plays no effect on GV, all of them exhibit the same trends. Compared with the widest beamwidth point in Figure 5, we can easily discover that the maximum beamwidth occurs at the point near zero GV.

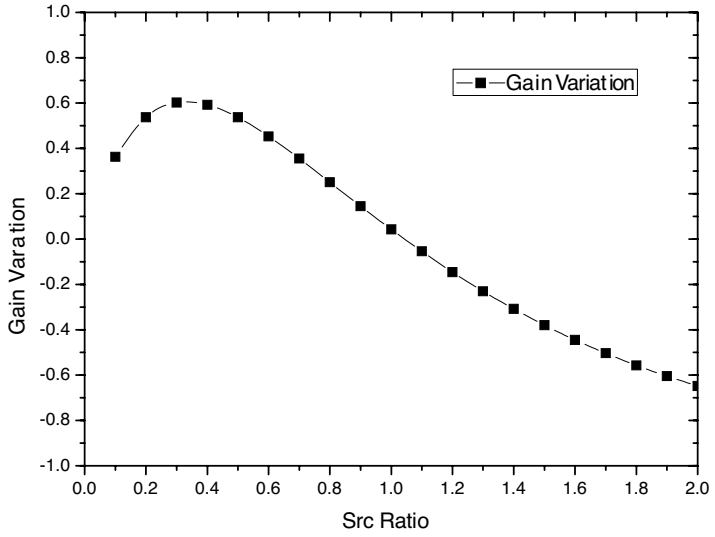

Figure 8. Variation of gain under different input magnitudes.

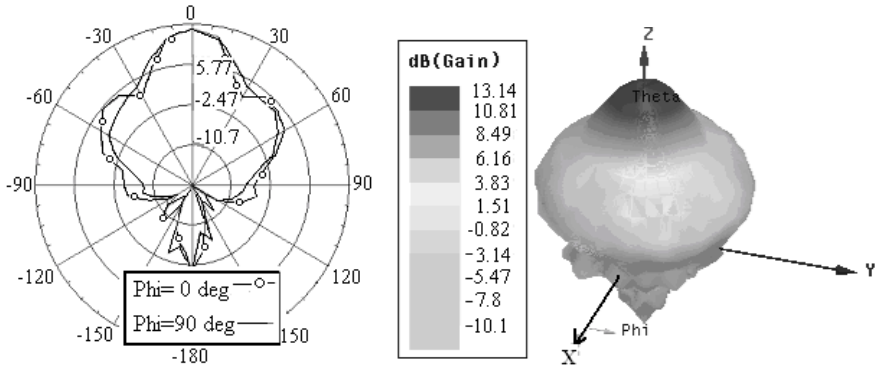

Figure 9. Radiation characteristic of the compensated crossed-dipole in the far-field.

Figure 9 shows the radiation pattern of the far-field. As can be seen, the maximum radiation intensity is about 14 dB, also the directivity is pretty well. Also the radiation is symmetrical around the boresite direction and the directivity of the antenna is not distorted.

5. CONCLUSION

The crossed-dipole excited reflector antenna presented in this paper exhibits a wider beamwidth and lower reflectance after using a paraboloidal photonic crystals compensation at 12.45 GHz. The discrimination of cross-polarization is reduced significantly. This crossed-dipole excited reflector can produce a pencil beam with a higher gain, low side lobes and good cross-polarization discrimination. It can be used as a feed to a larger reflector antenna as in a dual reflector antenna system, where the cross-polarization characteristics of the feed antenna are critical for the main reflector to produce well behaved radiations. The presented compensation technique exhibits distinguished performance to enhance it. In the future works, the combined optimization of the reflector and compensator will be studied for shaped reflector antennas to generate a better performance.

ACKNOWLEDGMENT

Thanks for the support provided by the National Science Council of R.O.C. for the funding support (NSC-97-2218-E-161-002) and the National High Technology Research and Development Project of China (NO. 2006AA01Z246).

REFERENCES

1. Manteghi, M. and Y. Rahmat-Samii, "On the characterization of a reflector Impulse Radiating Antenna (IRA) — Full-wave analysis and measured results," *IEEE Transactions on Antennas and Propagation*, Vol. 54, No. 3, 812–822, 2006.
2. Wang, A. and W. V. T. Ruscht, "Considerations on designing single- and dual-reflector antennas for efficient narrow pulse radiation," *IEEE Antennas and Propagation Society International Symposium*, Vol. 1, 62–65, 1994.
3. Rahmat-Samii, Y., D.-W. Duan, D. V. Giri, and L. F. Libelo, "Canonical examples of reflector antennas for high-power microwave applications," *IEEE Transactions on Electromagnetic Compatibility*, Vol. 34, No. 3, 197–205, 1992.

4. Liu, W. C. and P.-C. Kao, "Design of a probe-fed H-shaped microstrip antenna for circular polarization," *J. of Electromagn. Waves and Appl.*, Vol. 21, No. 7, 857–864, 2007.
5. Zandi, O., Z. Atlasbaf, and K. Forooraghi, "Flat multilayer dielectric reflector antennas," *Progress In Electromagnetics Research*, PIER 72, 1–19, 2007.
6. Pozar, M., *Microwave Engineering*, 3rd edition, John Wiley, 2005.
7. Button, M. D., "A robust and portable reflector antenna," *IEE Seminar on Satellite Services and the Internet*, 6/1–6/2, 2000.
8. Capozzoli, 8. A. and G. D'Elia, "Global optimization: Applications to advanced reflector antennas synthesis and diagnosis techniques," *Progress In Electromagnetics Research*, PIER 56, 195–232, 2006.
9. Saleh, E. A., *Fundamentals of Photonics*, Malvin Carl Teich, Eiley, 1991.
10. Rojas, J. A., J. Alpuente, P. Lpez-Esp, and P. Garcia, "Accurate model of electromagnetic wave propagation in unidimensional photonic crystals with defects," *J. of Electromagn. Waves and Appl.*, Vol. 21, No. 8, 1037–1051, 2007.
11. Villa-Villa, F., J. Gaspar-Armenta, and A. Mendoza-Suár, "Surface modes in one dimensional photonic crystals that include left handed materials," *J. of Electromagn. Waves and Appl.*, Vol. 21, No. 4, 485–499, 2007.
12. Yang, R., Y.-J. Xie, P. Wang, and T. Yang, "Conjugate left- and right-handed material bilayered substrates qualify the subwavelength cavity resonator microstrip antennas as sensors," *J. of Electromagn. Waves and Appl.*, Vol. 20, No. 15, 2113–2122, 2006.
13. Kasap, S. O., *Optoelectronics and Photonics*, Prentic Hall, 2001.
14. Terada, M., N. Bludworth, J. Moore, et al., "Deployable reflector system for satellite applications," *SBMO/IEEE MTT-S International Conference on Microwave and Optoelectronics*, 647–649, 2005.
15. Brown, E. R., C. D. Parker, and Yablonovitch, "Radiation properties of a planar antenna on a photonic-crystal substrate," *J. Opt. Soc. Am.*, Vol. B10, 404–407, 1993.
16. Busch, K., N. Vats, S. John, and B. C. Sanders, "Radiating dipoles in photonic crystals," *Phys. Rev.*, Vol. E62, No. 3, 4251–4260, 2000.
17. Balanis, C. A., *Antenna Theory*, 3rd edition, John Wiley, 1997.
18. Naghshvarian-Jahromi, M., "Novel Ku band fan beam reflector

back array antenna," *Progress In Electromagnetics Research Letters*, Vol. 3, 95–103, 2008.

19. Karimkashi, S. and J. Rashed-Mohassel, "Blockage minimization in symmetric dual-reflector antennas for different edge taper values," *J. of Electromagn. Waves and Appl.*, Vol. 20, No. 4, 5059–514, 2006.
20. Joardar, S. and A. B. Bhattacharya, "Two new ultra wideband dual polarized antenna-feeds using planar log periodic antenna and innovative frequency independent reflectors," *J. of Electromagn. Waves and Appl.*, Vol. 20, No. 11, 14659–1479, 2006.
21. Aissaoui, M., J. Zaghdoudi, M. Kanzari, and B. Rezig, "Optical properties of the quasi-periodic one-dimensional generalized multilayer Fibonacci structures," *Progress In Electromagnetics Research*, PIER 59, 69–83, 2006.
22. Kedar, A. and U. K. Revankar, "Parametric study of flat sandwich multilayer radome," *Progress In Electromagnetics Research*, PIER 66, 253–265, 2006.
23. Asole, F., L. Deias, and G. Mazzarella, "A flexible full-wave analysis of multilayered AMC using an aperture oriented approach," *J. of Electromagn. Waves and Appl.*, Vol. 21, No. 14, 2059–2072, 2007.
24. Xia, L., C.-F. Wang, L.-W. Li, P.-S. Kooi, and M.-S. Leong, "Resonant behaviours of microstrip antenna In multilayered media: An efficient full-wave analysis," *Progress In Electromagnetics Research*, PIER 31, 55–67, 2001.
25. Sounas, L., N. V. Kantartzis, and T. D. Tsiboukis, "Optimized ADI-FDTD analysis of circularly polarized microstrip and dielectric resonator antennas," *IEEE Microw. Wireless Compon. Lett.*, vol. 16, No. 2, 63–65, 2006.
26. Kishk, A. A., X. Zhang, A. W. Glisson, and D. Kaifez, "Numerical analysis of stacked dielectric resonator antennas excited by a coaxial probe for wideband applications," *IEEE Trans. Antennas Propag.*, Vol. 51, No. 8, 1996–2006, Aug. 2003.
27. Wilson, J. and J. Hawkes, *Optoelectronics*, 3rd edition, Prentice Hall, Europe, 1998.